Flood Inundation Assessment on Agricultural Land: Integrating High Spatial Resolution Sentinel Data with LiDAR DEM

Tran, T. P. and Nguyen, D. L.*
Faculty of Natural Resources and Environment, Vietnam National University of Agriculture, Vietnam
E-mail: nguyenducloc@vnua.edu.vn*
**Corresponding Author*

DOI: https://doi.org/10.52939/ijg.v21i3.3997

Abstract
Accurate flood inundation assessment is crucial for disaster management and agricultural resilience. This study integrates Sentinel-1 SAR, Sentinel-2 optical imagery, and high-resolution LiDAR DEM to develop a rapid flood mapping framework. Unlike traditional hydrodynamic models, we apply an image ratio method for flood extent detection and the Floodwater Depth Estimation Tool (FwDET) for flood depth mapping. The methodology was tested in Dien Chau district, Vietnam, where 6,917.55 ha of land was inundated, predominantly affecting paddy rice fields (6,369.05 ha submerged). The FwDET-derived flood depth map indicated a maximum depth of 3.14 m, with shallow flooding (0–0.5 m) being the most common. A Sentinel-2-based land use map achieved 93.05% accuracy (Kappa = 0.90), confirming its reliability for agricultural impact assessment. This study provides a cost-effective and scalable approach for flood mapping, supporting disaster response, land use planning, and agricultural resilience in flood-prone areas.

Keywords: Flood Depth Estimation Tool (FwDET), Flood Mapping, LiDAR DEM, Sentinel-1 SAR, Sentinel-2.

1. Introduction

Flooding is one of the most devastating natural disasters, with significant impacts agricultural land [1]. In recent years, the frequency and intensity of flood events have increased due to climate change and land use alterations [2], making flood management and mitigation essential. Agricultural land, in particular, is highly vulnerable to floods, as even short periods of inundation can lead to substantial economic losses by damaging crops and reducing productivity.

Accurate flood inundation assessment is critical for disaster response, land use planning, and agricultural management. Traditional flood mapping methods have relied on optical satellite imagery and hydrological models [3], but these approaches often face limitations, particularly in regions with frequent cloud cover and and require complex data. The integration of radar-based remote sensing data and high-resolution digital elevation models (DEM) provides a promising solution to these challenges.

Sentinel-1 Synthetic Aperture Radar (SAR) data offers high spatial resolution and the ability to capture flood events regardless of weather conditions [4], making it ideal for flood mapping. Meanwhile, highly precise digital elevation models, such as LiDAR-based DEMs, can accurately represent terrain features and improve the detection of floodwater depths and extents. By combining these advanced technologies, it is possible to generate detailed and reliable flood inundation maps, particularly for sensitive areas like agricultural land.

Modeling flood depth is a challenging task, typically carried out using hydrologic and hydraulic models such as MIKE-FLOOD [5] or HEC-RAS [6]. Machine learning has also been applied to predict flood depth, either independently [7] or in combination with hydraulic models [8]. These methods give accurate results but need a lot of complex data so could not applied for many regions. While these methods can produce accurate results, they require large amounts of complex data, making them difficult to apply in many regions. To address this, the Floodwater Depth Estimation Tool (FwDET) was developed to calculate water depth from DEM and flood extents extracted from satellite imagery [9]. In 2020, FwDET was integrated into Google Earth Engine (GEE) and has been applied in various flood studies [10] and [11].

This study aims to develop a new, efficient, and scalable flood mapping and depth estimation framework by integrating Sentinel-1 SAR and high-resolution LiDAR DEM within Google Earth Engine (GEE). Unlike traditional hydrodynamic models that require complex input data and intensive computation, this research introduces an automated, data-driven approach that enables rapid flood extent detection and water depth estimation. Specifically, the study (1) enhances flood extent mapping using Sentinel-1 SAR and an optimized image ratio method, (2) improves flood depth estimation by applying FwDET with high-resolution LiDAR DEM, (3) validates agricultural flood impacts using a high-accuracy land use map from Sentinel-2, and (4) demonstrates the efficiency of cloud-based processing for large-scale flood mapping and disaster response.

By developing a computationally efficient and scalable flood mapping approach, this research supports flood mitigation, crop management, and land use planning, offering a cost-effective alternative to traditional hydrodynamic modeling.

2. Materials and Methods

2.1 Study Area

Dien Chau is located in the eastern part of Nghe An province (Figure 1). It borders the East Sea to the east, Yen Thanh district to the west, Quynh Luu district to the north, and Nghi Loc district to the south. The central area has relatively flat terrain, making it ideal for agriculture, while the northern and southern regions have high hills, suitable for forestry. The average temperature ranges from 22°C to 25°C, with humidity exceeding 80%. Located in a monsoon tropical climate zone, the district experiences high rainfall, mostly concentrated between August and October, with the highest recorded value of 360.2 mm occurring in September (Figure 2).

Figure 1: Dien Chau, Nghe An province, Vietnam

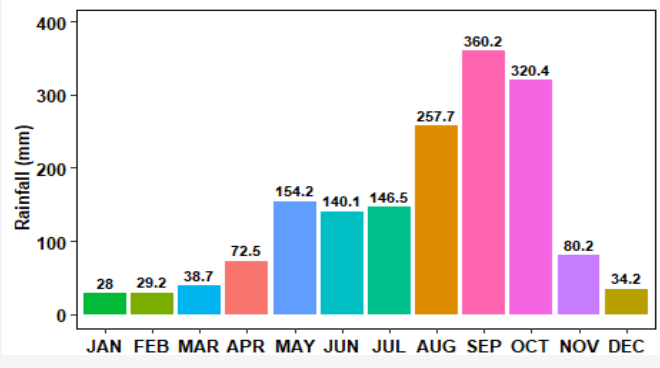

Figure 2: Monthly average rainfall from 2010 to 2020

2.2 Data Used

2.2.1 Sentinel 1 SAR data

Detecting water on the Earth's surface is a crucial task in natural resources monitoring through satellite imagery. Analyzing temporal images allows for the identification of changes in water surfaces over time. Compare to optical images, radar images has proven their advantage in water surfaces detection: penetrating cloud cover and operating in various weather conditions [12]. This makes radar imagery a valuable tool for accurate monitoring of water surfaces, complementing the capabilities of optical images.

Twin C - band radar satellite operated ESA, Sentinel - 1A and Sentinel - 1B, provide free SAR imagery data with time intervals of 6 days [13]. The high spatial resolution of 10 meter allows them to accurately monitor the changes in the earth surfaces, especially water body. They was used as input data for studies related to water surface changes[14][15] and [16]. VV polarization has been reported to produce more accurate flood maps than VH when using Sentinel-1 for flood mapping [17]. In this study, VV polarization from two Sentinel-1 Ground Range Detected (GRD) images, acquired on September 24 and October 30, 2020, was used to detect floodwater in Dien Chau district.

2.2.2 Sentinel 2 optical data

Sentinel-2, a free optical remote sensing data, has been widely used for land cover mapping. It consists of two satellites, Sentinel-2A and Sentinel-2B, launched in 2015 and 2017, respectively. Sentinel-2 imagery has been employed in both global and local land use studies [18] and [19]. Similar to other optical remote sensing data, Sentinel-2 imagery is significantly affected by weather conditions, particularly cloud cover. To mitigate this issue, an effective solution has been introduced, cloud-free annual composite. A previous study demonstrated that optical data composites are more accurate than Synthetic Aperture Radar (SAR) in wetland mapping [20]. Similarly, monthly composites of Sentinel-2 optical data have also been shown to provide higher accuracy than Sentinel-1 data in crop mapping [21]. This study utilizes cloud-free annual composite of Sentinel-2 imagery to develop a 2020 land use map for Dien Chau district Figure 3(a).

2.2.3 Highly precise LiDAR-based DEM

A Digital Elevation Model (DEM) is crucial for flood analysis, serving as essential input data for flood susceptibility [22] and [23] and flood depth mapping [24] and [25]. DEMs can be developed from topographical information collected via UAV [26], LiDAR [27], or satellite imagery [28] and [29]. Several studies have demonstrated that LiDAR-based DEMs are the most accurate for flood analysis [30][31] and [32]. This study used a highly precise LiDAR-based DEM at a 1m x 1m resolution, established in 2016 by the Vietnam Department of Surveying, Mapping and Geographic Information (https://www.bandovn.vn/vi/dem-1mx1m-35). The DEM was resampled to 10m x 10m to align with the spatial resolution of Sentinel-1 and Sentinel-2 imagery.

2.3 Land Use Mapping

Five main land use types - Permanent Water, Annual Crops, Paddy Rice, Residential Area, and Forest - were identified from a yearly composite of Sentinel-2 imagery. A field survey was conducted to collect the coordinates of 60 points for each land use type. These points were randomly divided into two subsets: 40 points for training and 20 points for testing. The points served as reference data for creating sample polygons representing the land use classes. A Support Vector Machine (SVM) with a radial basis function (RBF) kernel was used to classify the composite image. This algorithm has been shown to outperform Random Forest and Neural Networks for land cover classification [33] and [34]. To assess the accuracy of land use map, several indices were used: Overall Accuracy (OA), Kappa coefficient (K), User's Accuracy (UA), and Producer's Accuracy (PA).

2.4 Flood Inundation Mapping

Before the availability of free radar imagery, flood maps were typically developed using optical satellite imagery, such as Landsat [35], LISS III [36], or MODIS [37]. However, optical remote sensing data were often affected by bad weather conditions [38], which delayed the estimation of flooded areas by several days after flood events [39]. Today, Sentinel-1 SAR imagery is freely available and offers significant advancements in flood detection, with its high spatial resolution (10m) and frequent revisit time (6 days). Several methods were applied to detect flood inundation water for radar imagery, including thresholding, change detection, unsupervised classification and supervised classification [15]. This study used the change detection approach with the image rationing method. After image correction, the ratio is calculated for each pixel of pre-flood image and post-flood image by Equation 1:

$$R(x,y) = \frac{S_2(x,y)}{S_1(x,y)}$$

Equation 1

Where:

$R(x,y)$ is ratio value of each pixel;
$S_1(x,y)$: pixel value of pre-flood image;
$S_2(x,y)$: pixel value of post-flood image.

A threshold of 1.25, as suggested by UN-SPIDER (2022), was used to distinguish between water and non-water areas. Additionally, LiDAR DEM data were used to remove dark pixels with slope angles greater than 10°, where shadows and dark surface noise in SAR images could affect the determination of flood extent. The image rationing approach is simple yet effective in highlighting significant changes, especially flooding.

2.5 Flood Depth Estimation

Flood depth is typically estimated using hydrological and hydraulic models [40] and [41]. These methods require complex data inputs and a deep understanding of hydrological processes. Recently, researchers have used machine learning algorithms to estimate flood depth however there is a high bias of predicted flood depth value. This study used Floodwater Depth Estimation Tool (FwDET) integrated in Google Earth Engine to extract floodwater depth map from flood extents and LiDAR DEM. The tool was developed in 2017 and integrated into Google Earth Engine in 2020 [42] and [43]. It is designed to calculate water depth using a remote sensing-based inundation extent layer and a Digital Elevation Model (DEM). Its algorithm follows five key steps [42]: (1) Identifying boundary cells: The algorithm first identifies the boundary cells of the flooded area based on the inundation extent, (2) Extracting elevation of boundary cells: It extracts the elevation values of these boundary cells from the DEM, (3) Assigning elevation to flooded domain cells: The elevation of the nearest boundary cell is assigned to each cell within the flooded area, (4) Calculating floodwater depth: Water depth is determined by subtracting the DEM elevation from the assigned flood elevation, and (5) Smoothing: A filtering step is applied to refine depth estimates and reduce spatial artifacts. The tool can be downloaded at https://github.com/csdms-contrib/fwdet.

An evaluation of FwDET performance was conducted at Brazos River, Texas, and St. Vrain Creek, Colorado [42]. Using a 10 m DEM at Brazos River, the average absolute difference between floodwater depths estimated by FwDET and the iRIC-FaSTMECH hydraulic model was 0.37 m. At St. Vrain Creek, where a 1 m Lidar DEM was used, the difference was 0.38 m. Additionally, a trial using FwDET 2.0 was conducted in a coastal area at Portsmouth and Norfolk, Virginia, USA, with a 1 m LiDAR DEM [9]. The results showed an average difference of 0.18 m between the floodwater depths estimated by FwDET 2.0 and a hydrodynamic model. A separate study on flood depth estimation in a coastal area of Vietnam found that the mean difference between FwDET-based depth estimates and 717 field observations was 0.126 m [11]. These validations demonstrate that FwDET is a reliable tool for estimating flood depth in coastal areas, including regions such as Dien Chau district.

2.6 Flood Damage Assessment

ArcGIS software was used to analyze the flood extent across communes and assess flood depth on agricultural land in Dien Chau district. For the first task, the flood map was overlaid with the commune boundary map. For the second task, the flood depth map was overlaid with agricultural land, including paddy fields and annual crops, which were extracted from the land use map. The flow chart of the study is presented in Figure 4.

3. Results and Discussion

3.1 Land Use Map

The land use classification results are presented in Figure 3(b). Forested areas are primarily located in the northern and southern parts of the district, where the terrain consists of high hills. The central region, characterized by flat plains ideal for agriculture, is predominantly used for paddy rice cultivation and annual crops. Residential areas are evenly distributed in the central part, close to agricultural zones. To assess the accuracy of the land use map, twenty polygon samples for each class were created using in-situ data. The results in Table 1 show that the map is highly accurate, with an overall accuracy of 93.05% and a Kappa coefficient of 0.90. Paddy rice had the highest classification accuracy, with a producer's accuracy of 1 and a user's accuracy of 0.94. Although annual crops had the lowest accuracy, it was still reasonably good, with both producer's and user's accuracies at 0.83. The remaining classes were accurately classified, with both producer's and user's accuracies exceeding 0.90.

According to the calculation results, paddy rice is the dominant land use type, covering 13,546.15 ha, which accounts for 44.40% of the total area. It is followed by forest, annual crops, and residential areas, with areas of 5,203.51 ha, 5,186.34 ha, and 5,121.60 ha, respectively. The smallest land use category is water, covering 1,450.96 ha, or 4.76% of the total area.

Table 1: Confusion matrix and accuracy indices

		Land use map					Row Total	Producer's Accuracy
		Pemanent Water	Annual Crop	Paddy Rice	Residential Area	Forest		
Reference Data	Pemanent Water	211	0	15	0	0	226	0.93
	Annual Crop	0	266	7	21	27	321	0.83
	Paddy Rice	0	0	348	0	0	348	1.00
	Residential Area	0	22	0	823	34	879	0.94
	Forest	0	33	0	17	566	616	0.92
Column Total		211	321	370	861	627	OA = 93.05%	
User's Accuracy		1	0.83	0.94	0.96	0.90	Kappa = 0.90	

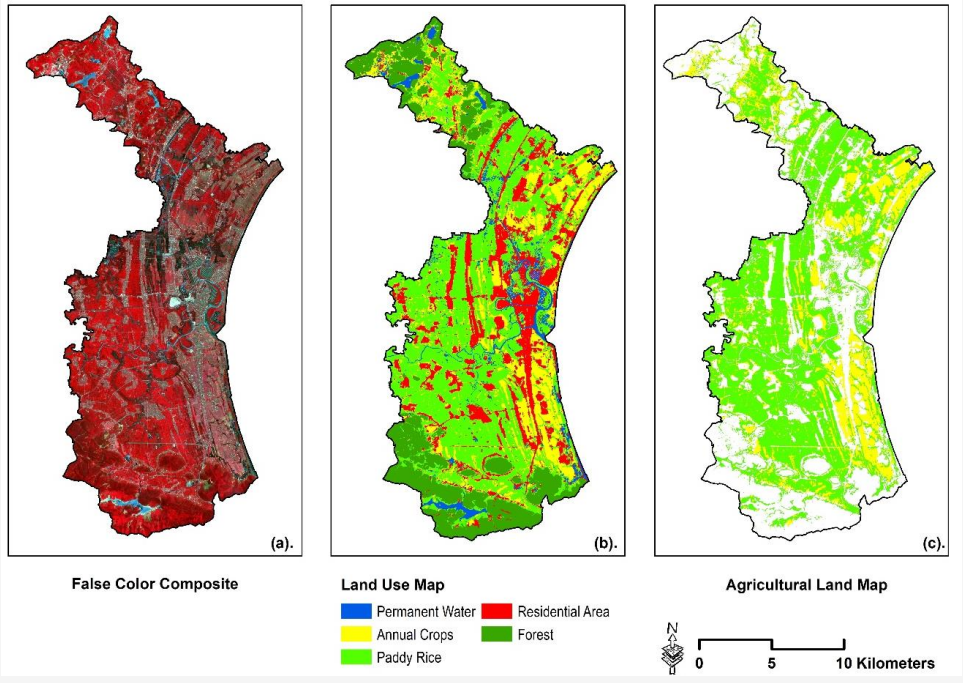

Figure 3: Optical imagery of Dien Chau and its extractions:
(a) false color composite (b) land use map (c) agricultural land map

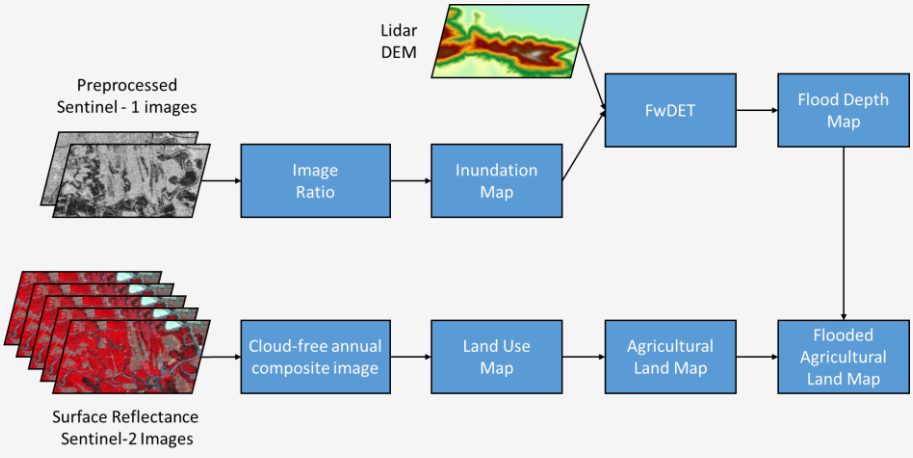

Figure 4: Detection of agricultural land affected by flood

3.2 Flood Mapping and Damage Assessment

Sentinel-1 images of pre- and post-flood events are presented in Figures 5(a) and 5(b). The ratio image, which is obtained by dividing the post-flood Sentinel-1 image by the pre-flood image, is displayed in Figure 5(c). In the post-flood image, floodwater appears dark due to the low backscatter intensity characteristic of SAR imagery. In contrast, the floodwater appears white in the ratio image, indicating a significant change in pixel values resulting from flooding. A threshold of 1.25 was employed to classify the ratio image into two categories: floodwater and non-floodwater. The flood extent map presented in Figure 6(a) features a LiDAR DEM background with the floodwater overlaying the DEM. The calculation results shows that the total flooded area is 6917.55 ha. Notably, all communes of the district are flooded except Dien Chau town (Table 2).

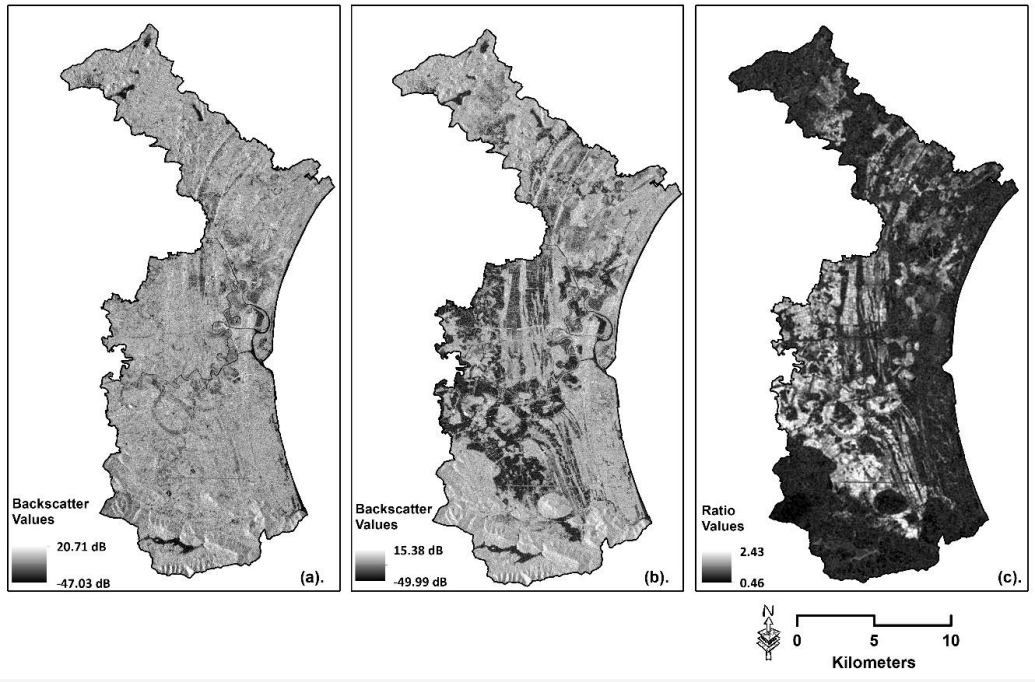

Figure 5: SAR imagery of Dien Chau (a) pre flood (b) post flood (c) ratio image

Table 2: Flooded area by communes in Dien Chau district

ID	Commune	Commune area (ha)	Flooded Area (ha)	% of the flooded area	ID	Commune	Commune area (ha)	Flooded area (ha)	% of the flooded area
1	Dien An	779.15	112.33	14.42	21	Dien Ngoc	278.35	20.70	7.44
2	Dien Bich	262.72	18.29	6.96	22	Dien Nguyen	554.90	295.74	53.30
3	Dien Binh	493.75	250.57	50.75	23	Dien Phong	383.78	55.68	14.51
4	Dien Cat	706.23	350.78	49.67	24	Dien Phu	3,343.03	349.36	10.45
5	Dien Doai	1,328.55	230.46	17.35	25	Dien Phuc	441.650	127.80	28.94
6	Dien Dong	559.56	309.23	55.26	26	Dien Quang	432.99	124.37	28.72
7	Dien Hai	520.71	120.87	23.21	27	Dien Tan	481.80	163.16	33.86
8	Dien Hanh	441.88	79.31	17.95	28	Dien Thai	635.97	362.30	56.97
9	Dien Hoa	421.48	102.55	24.33	29	Dien Thang	816.61	337.42	41.32
10	Dien Hoang	629.59	62.57	9.94	30	Dien Thanh	719.22	51.01	7.09
11	Dien Hong	645.90	152.33	23.58	31	Dien Thap	381.94	140.59	36.81
12	Dien Hung	533.04	2.72	0.51	32	Dien Thinh	839.66	20.65	2.46
13	Dien Kim	607.99	48.27	7.94	33	Dien Tho	840.02	456.54	54.35
14	Dien Ky	636.07	143.43	22.55	34	Dien Trung	1,371.51	23.60	1.72
15	Dien Lam	3,466.58	329.80	9.51	35	Dien Truong	881.59	188.95	21.43
16	Dien Lien	700.84	419.41	59.84	36	Dien Van	424.01	81.74	19.28
17	Dien Loc	728.80	276.93	38.00	37	Dien Xuan	368.31	168.09	45.64
18	Dien Loi	1,580.74	353.01	22.33	38	Dien Yen	1,326.96	282.96	21.32
19	Dien Minh	415.49	247.30	59.52	39	TT Dien Chau	106.56	0.00	0.00
20	Dien My	420.63	56.74	13.49		**Total (ha)**	**30,508.56**	**6,917.55**	**22.67**

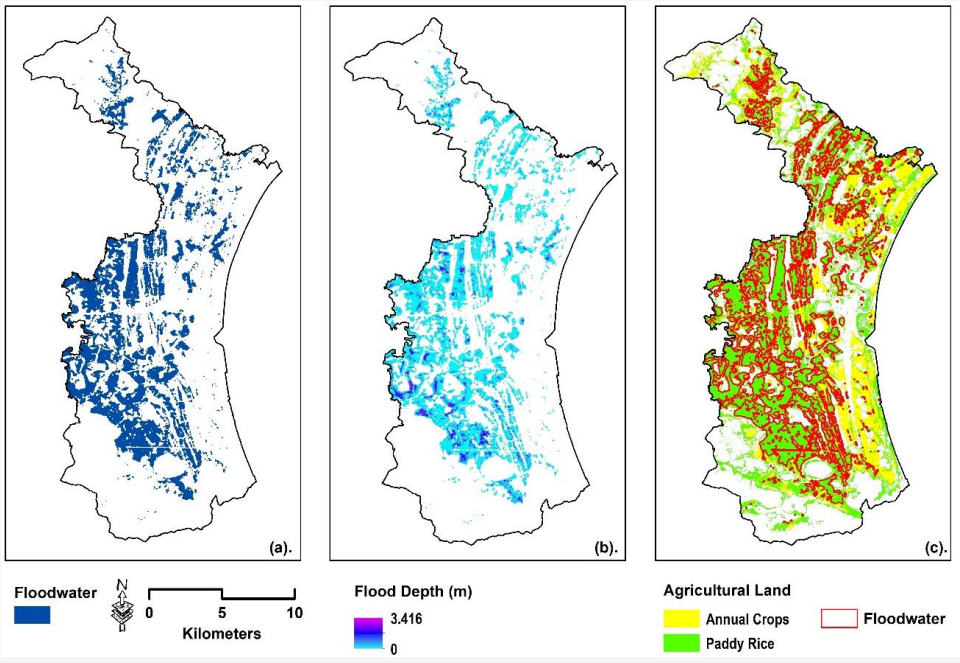

Figure 6: Thematic maps: (a) flood map (b) flood depth map (c) overlay flood map on agricultural land map

Table 3: Flooded area of annual crops and paddy rice

Flood Depth (m)	Annual Crops	Paddy Rice	Area (ha)
0.0-0.5	175.62	5,923.40	6,099.02
0.5-1.0	2.94	343.71	346.65
1.0-1.5	0.80	78.61	79.41
1.5-2.0	1.83	16.82	18.65
2.0-2.5	0.00	5.49	5.49
2.5-3.0	0.00	0.82	0.82
3.0-3.4	0.00	0.20	0.20
Total flooded area (ha)	**181.19**	**6,369.05**	**6,550.24**
Total area (ha)	**5,186.34**	**13,546.15**	**18,732.49**
Percentage (%)	**3.49**	**47.02**	**34.97**

The commune has the highest flooded area is Dien Tho, 456.54 ha, which was followed by Dien Lien commun, 419.41ha. The number of communes with flooded areas is distributed as follows: 6 communes in the 300 - 400 ha range, 6 in the 200 - 300 ha range, 12 in the 100 - 200 ha range, and 12 with less than 100 ha. Figure 6(b) illustrates the flood depth map calculated by FwDET using LiDAR DEM and flood extent data. The calculation results indicate that the maximum depth is 3.14 m. The areas with flood depths of 0 - 0.5 m, 0.5 - 1.0 m, 1.0 - 1.5 m, 1.5 - 2.0 m, 2.0 - 2.5 m, 2.5 - 3.0 m, and >3.0 m are 6,418.71 ha, 384.75 ha, 85.92 ha, 20.61 ha, 6.03 ha, 0.99 ha, and 0.54 ha, respectively. This flooded area primarily affects the agricultural zones of the communes.

Figure 6(c) represents flood depth map overlay the agricultural land map. Table 3 presents the flooded area of annual crops and paddy rice, categorized by various flood depths. The total area affected by flooding is 6,550.24 hectares, with paddy rice experiencing significantly higher flood impacts than annual crops. At depths of 0.0–0.5 m, floodwaters cover 5,923.40 ha of paddy rice, while the flooded area of annual crops accounts for only 175.62 ha. As flood depth increases, the area of annual crops affected by flooding decreases sharply, with minimal areas recorded at greater depths. For example, at depths of 0.5–1.0 m, annual crops are flooded across 2.94 ha, and this number continues to dwindle at deeper levels. Conversely, paddy rice remains affected even at greater depths, with 343.71 ha inundated at 0.5–1.0 m and several areas noted at depths of 2.5 m and even up to 3.4 m. This data highlights the vulnerability of agricultural areas to flooding and suggests that the government develop agricultural production plans and appropriate farming measures to mitigate the damage caused by floods to agricultural production.

4. Conclusions

This study successfully integrated Sentinel-1 SAR, Sentinel-2 optical imagery, and high-resolution LiDAR DEM to assess flood inundation and its impact on agricultural land in Dien Chau district. The land use classification achieved high accuracy with an overall accuracy of 93.05% and a Kappa coefficient of 0.90, confirming the effectiveness of Sentinel-2 imagery for land use mapping. Paddy rice cultivation was identified as the dominant land use, covering over 44% of the total area, primarily in low-lying central plains.

Flood mapping results revealed that 6,917.55 ha of the district was inundated, affecting all communes except Dien Chau town. Dien Tho commune experienced the most severe flooding, with 456.54 ha submerged. Flood depth analysis using the Floodwater Depth Estimation Tool (FwDET), combined with LiDAR DEM, estimated a maximum flood depth of 3.14 m, with shallow flooding (0–0.5 m) covering most of the affected area.

The FwDET tool within Google Earth Engine (GEE) provided a computationally efficient and scalable method for flood depth estimation. The results indicate that FwDET is a good alternative to traditional hydrodynamic models, especially in data-scarce regions. However, its accuracy is influenced by the quality of DEM data and the precision of flood extent delineation. Future enhancements could involve improving flood boundary extraction methods and integrating hydrodynamic modeling for better accuracy.

These findings highlight the vulnerability of agricultural land to flooding, particularly paddy rice fields, which suffered the most significant impact, with 6,369.05 ha submerged. This underscores the need for targeted flood mitigation strategies, including adaptive farming techniques, enhanced drainage infrastructure, and improved early warning systems. The methodology presented in this study can be applied to other flood-prone areas to support disaster response, agricultural planning, and land management. A limitation of this study is the lack of ground-based validation for flood depth. The accuracy of FwDET-derived flood depths was not verified using field measurements or in-situ water level data. Future studies should incorporate ground truthing to enhance validation and improve accuracy.

References

[1] Chau, V. N., Cassells, S. and Holland, J., (2015). Economic Impact upon Agricultural Production from Extreme Flood Events in Quang Nam, Central Vietnam. *Natural Hazards*, Vol.75 1747-1765. https://doi.org/10.1007/s11069-014-1395-x.

[2] Pal, S. C., Chowdhuri, I., Das, B., Chakrabortty, R., Roy, P., Saha, A. and Shit, M., (2022). Threats of Climate Change and Land Use Patterns Enhance the Susceptibility of Future Floods in India. *Journal of Environmental Management*, Vol. 305. https://doi.org/10.1016/j.jenvman.2021.114317.

[3] Khan, S. I., Hong, Y., Wang, J., Yilmaz, K. K., Gourley, J. J., Adler, R. F., Brakenridge, G. R., Policelli, F., Habib, S. and Irwin, D., (2011). Satellite Remote Sensing and Hydrologic Modeling for Flood Inundation Mapping in Lake Victoria Basin: Implications for Hydrologic Prediction in Ungauged Basins. *IEEE Transactions on Geoscience and Remote Sensing*, Vol.49, 85-95. https://doi.org/10.1007/s11069-014-1395-x10.1109/TGRS.2010.205751 3.

[4] Khamphilung, P., Konyai, S., Slack, D., Chaibandit, K. and Prasertsri, N., (2023). Flood Event Detection and Assessment using Sentinel-1 SAR-C Time Series and Machine Learning Classifiers Impacted on Agricultural Area, Northeastern, Thailand. *International Journal of Geoinformatics*, Vol. 19(6), 17–29. https://doi.org/10.52939/ijg.v19i6.2691.

[5] Kadam, P. and Sen, D., (2012). Flood Inundation Simulation in Ajoy River Using MIKE-FLOOD. *ISH Journal of Hydraulic Engineering*, Vol.18. 129-141. https://doi.org/10.1080/09715010.2012.695449.

[6] Alshammari, E., Abdul Rahman, A., Ranis, R., Abu Seri, N. and Ahmad, F. (2024). Investigation of Runoff and Flooding in Urban Areas based on Hydrology Models: A Literature Review. *International Journal of Geoinformatics*, Vol. *20*(1), 99–119. https://doi.org/10.52939/ijg.v20i1.3033.

[7] Wu, Z., Zhou, Y., Wang, H. and Jiang, Z., (2020). Depth Prediction of Urban Flood under Different Rainfall Return Periods Based on Deep Learning and Data Warehouse. *Science of The Total Environment*, Vol.716. https://doi.org/10.1016/j.scitotenv.2020.137077.

[8] Hosseiny, H., Nazari, F., Smith, V. and Nataraj, C., (2020). A Framework for Modeling Flood Depth Using a Hybrid of Hydraulics and Machine Learning. *Scientific Reports*, Vol.10. https://doi.org/10.1038/s41598-020-65232-5.

[9] Cohen, S., Raney, A., Munasinghe, D., Loftis, J. D., Molthan, A., Bell, J., Rogers, L., Galantowicz, J., Brakenridge, G. R., Kettner, A. J., Huang, Y. F. and Tsang, Y. P., (2019). The Floodwater Depth Estimation Tool (FwDET v2.0) for Improved Remote Sensing Analysis of Coastal Flooding. *Natural Hazards and Earth System Sciences*, Vol. 19, 2053-2065, https://doi.org/10.5194/nhess-19-2053-2019.

[10] Cohen, S., Peter, B. G., Haag, A., Munasinghe, D., Moragoda, N., Narayanan, A. and May, S., (2022). Sensitivity of Remote Sensing Floodwater Depth Calculation to Boundary Filtering and Digital Elevation Model Selections. *Remote Sensing*, Vol. 14. https://doi.org/10.3390/rs14215313.

[11] Liou, Y. A. and Hoang, D. V., (2024). Improved Flood Depth Estimation with SAR Image, Digital Elevation Model, and Machine Learning Schemes. *Journal of Hydrology: Regional Studies*, Vol. 53. https://doi.org/10.1016/j.ejrh.2024.101775.

[12] Gupta, D. K., Prashar, S., Singh, S., Srivastava, P. K. and Prasad, R., (2022). Chapter 1 - Introduction to RADAR Remote Sensing. *Radar Remote Sensing*, 3-27. https://doi.org/10.1016/B978-0-12-823457-0.00018-5.

[13] Zhang, M., Chen, F., Tian, B., Liang, D. and Yang, A., (2020). High-Frequency Glacial Lake Mapping Using Time Series of Sentinel-1A/1B SAR Imagery: An Assessment for the Southeastern Tibetan Plateau. *International Journal of Environmental Research and Public Health*, Vol.17. https://doi.org/10.3390/ijerph17031072.

[14] Shen, G., Fu, W., Guo, H. and Liao, J., (2022). Water Body Mapping Using Long Time Series Sentinel-1 SAR Data in Poyang Lake. *Water*, Vol.14. https://doi.org/10.3390/w14121902.

[15] Tazmul Islam, M. and Meng, Q., (2022). An Exploratory Study of Sentinel-1 SAR for Rapid Urban Flood Mapping on Google Earth Engine. *International Journal of Applied Earth Observation and Geoinformation*, Vol.113. https://doi.org/10.1016/j.jag.2022.103002.

[16] Tupas, M. E., Roth, F., Bauer-Marschallinger, B. and Wagner, W., (2023). An Intercomparison of Sentinel-1 Based Change Detection Algorithms for Flood Mapping. *Remote Sensing*, Vol.15. https://doi.org/10.3390/rs15051200.

[17] Abbasi, M., Shah-Hosseini, R. and Aghdami-Nia, M., (2023). Sentinel-1 Polarization Comparison for Flood Segmentation Using Deep Learning. *Proceedings*, Vol. 87. https://doi.org/10.1007/s11069-014-1395-x10.3390/IECG2022-14069.

[18] Arunplod, C., Phonphan, W., Wongsongja, N., Utarasakul, T., Niemmanee, T., Daraneesrisuk, J. and Thongdara, R. (2023). Spatial Dynamics Evolution of Land use for the Study of the Local Traditional Living Changes. *International Journal of Geoinformatics*, Vol. 19(4), 37–49. https://doi.org/10.52939/ijg.v19i4.2635.

[19] Nguyen, H. T., Doan, T. M., Tomppo, E. and McRoberts, R. E., (2020). Land Use/Land Cover Mapping Using Multitemporal Sentinel-2 Imagery and Four Classification Methods-A Case Study from Dak Nong, Vietnam. *Remote Sensing*, Vol.12. https://doi.org/10.3390/rs12091367.

[20] Mahdianpari, M., Salehi, B., Mohammadimanesh, F., Homayouni, S. and Gill, E., (2019). The First Wetland Inventory Map of Newfoundland at a Spatial Resolution of 10 m Using Sentinel-1 and Sentinel-2 Data on the Google Earth Engine Cloud Computing Platform. *Remote Sensing*, Vol.11. https://doi.org/10.3390/rs11010043.

[21] Luo, C., Liu, H. J., Lu, L. P., Liu, Z. R., Kong, F.C. and Zhang, X. L., (2021). Monthly Composites from Sentinel-1 and Sentinel-2 Images for Regional Major Crop Mapping with Google Earth Engine. *Journal of Integrative Agriculture*, Vol. 20, 1944-1957. https://doi.org/10.1016/S2095-3119(20)63329-9.

[22] Mohd Rasu, M., Suhandri, H., Khalifa, N., Abdul Rasam, A. and Hamid, A., (2023). Evaluation of Flood Risk Map Development through GIS-Based Multi-Criteria Decision Analysis in Maran District, Pahang - Malaysia. *International Journal of Geoinformatics*, Vol. 19(10), 1–16. https://doi.org/10.52939/ijg.v19i9.2873.

[23] Kumne, W. and Samanta, S., (2023). Geospatial Mapping of Inland Flood Susceptibility Based on Multi-Criteria Analysis – A Case Study in the Final Flow of Busu River Basin, Papua New Guinea. *International Journal of Geoinformatics*, Vol. 19(6), 31–48. https://doi.org/10.52939/ijg.v19i6.2693.

[24] Elkhrachy, I., (2022). Flash Flood Water Depth Estimation Using SAR Images, Digital Elevation Models, and Machine Learning Algorithms. *Remote Sensing*, Vol. 14. https://doi.org/10.3390/rs14030440.

[25] Hao, C., Yunus, A. P., Siva Subramanian, S. and Avtar, R., (2021). Basin-wide Flood Depth and Exposure Mapping from SAR Images and Machine Learning Models. *Journal of Environmental Management,* Vol. 297. https://doi.org/10.1016/j.jenvman.2021.113367

[26] Aziz, M., Pa'suya, M., Talib, N., Din, A., Hashim, S. and Ramli, M., (2023). Vertical Accuracy Assessment of Improvised Global Digital Elevation Models (MERIT, NASADEM, EarthEnv) Using GNSS and Airborne IFSAR DEM. *International Journal of Geoinformatics*, Vol. 19(12), 65–82. https://doi.org/10.52939/ijg.v19i12.2979.

[27] Jifroudi, H., Mansor, S. and Pradhan, B. (2022). Rule-based Learning Techniques to Derive Automated Digital Terrain Model Using Airborne LiDAR Data. *International Journal of Geoinformatics*, Vol. 18(6), 33–46. https://doi.org/10.52939/ijg.v18i6.2459.

[28] Bhushan, S., Shean, D., Alexandrov, O. and Henderson, S., (2021). Automated Digital Elevation Model (DEM) Generation from Very-High-Resolution Planet SkySat Triplet Stereo and Video Imagery. *ISPRS Journal of Photogrammetry and Remote Sensing*, Vol. 173, 151-165. https://doi.org/10.1016/j.isprsjprs.2020.12.012.

[29] Palamà, R., Monserrat, O., Crippa, B., Crosetto, M., Bru, G., Ezquerro, P. and Bejar-Pizarro, M., (2023). Radargrammetry DEM Generation Using High-Resolution SAR Imagery Over La Palma During the 2021 Cumbre Vieja Volcanic Eruption. *IEEE Geoscience and Remote Sensing Letters,* Vol. 20, 1-5, https://doi.org/10.1109/LGRS.2023.3238182.

[30] Casas, A., Benito, G., Thorndycraft, V. R. and Rico, M., (2006). The Topographic Data Source of Digital Terrain Models as a Key Element in the Accuracy of Hydraulic Flood Modelling. *Earth Surface Processes and Landforms,* Vol. 31, 444-456, https://doi.org/10.1002/esp.1278.

[31] Schumann, G., Matgen, P., Cutler, M. E. J., Black, A., Hoffmann, L. and Pfister, L., (2008). Comparison of Remotely Sensed Water Stages from LiDAR, Topographic Contours and SRTM. *ISPRS Journal of Photogrammetry and Remote Sensing*, Vol. 63, 283-296. https://doi.org/10.1016/j.isprsjprs.2007.09.004.

[32] Wang, Y. and Zheng, T., (2005). Comparison of Light Detection and Ranging and National Elevation Dataset Digital Elevation Model on Floodplains of North Carolina. *Natural Hazards Review*, Vol. 6, 34-40. https://doi.org/10.1061/(ASCE)1527-6988(2005)6:1(34).

[33] Dabija, A., Kluczek, M., Zagajewski, B., Raczko, E., Kycko, M., Al-Sulttani, A. H., Tardà, A., Pineda, L. and Corbera, J., (2021). Comparison of Support Vector Machines and Random Forests for Corine Land Cover Mapping. *Remote Sensing*, Vol.13. https://doi.org/10.3390/rs13040777.

[34] Zagajewski, B., Kluczek, M., Raczko, E., Njegovec, A., Dabija, A. and Kycko, M., (2021). Comparison of Random Forest, Support Vector Machines, and Neural Networks for Post-Disaster Forest Species Mapping of the Krkonoše/Karkonosze Transboundary Biosphere Reserve. *Remote Sensing*, Vol. 13. https://doi.org/10.3390/rs13132581.

[35] Ngo, A., Grivel, S., Nguyen, T., and Nguyen, T. (2023). Impact Assessment of Land Use and Land Cover Change on the Runoff Changes on the Historical Flood Events in the Laigiang River Basin of the South Central Coast Vietnam. *International Journal of Geoinformatics*, Vol. 19(10), 51–63. https://doi.org/10.52939/ijg.v19i9.2881.

[36] Jain, S. K., Singh, R. D., Jain, M. K. and Lohani, A. K., (2005). Delineation of Flood-Prone Areas Using Remote Sensing Techniques. *Water Resources Management,* Vol.19, 333-34, https://doi.org/10.1007/s11269-005-3281-5.

[37] Brakenridge, R. and Anderson, E., (2006). *MODIS-based Flood Detection, Mapping and Measurement: The Potential for Operational Hydrological Applications*. Marsalek, J., Stancalie, G., Balint, G. (eds) Transboundary Floods: Reducing Risks through Flood Management. Nato Science Series: IV: Earth and Environmental Sciences, Vol. 72. https://doi.org/10.1007/1-4020-4902-1_1.

[38] Lin, L., Di, L., Yu, E. G., Kang, L., Shrestha, R., Rahman, M. S., Tang, J., Deng, M., Sun, Z., Zhang, C. and Hu, L., (2016). *A Review of Remote Sensing in Flood Assessment*. 2016 Fifth International Conference on AGRO-Geoinformatics, 18-20 July 2016, Tianjin, China, https://doi.org/10.1109/Agro-Geoinformatics.2016.7577655.

[39] Muttaqin, K., Maulita, M., Fitria, L., Ihsan, A. and Mulya, R., (2023). Mapping Flood-Prone Areas Based Geographic Information System Using Composite Mapping Analysis. *International Journal of Geoinformatics*, Vol. 19(12), 93–105. https://doi.org/10.52939/ijg.v19i12.2983.

.

[40] Nogherotto, R., Fantini, A., Raffaele, F., Di Sante, F., Dottori, F., Coppola, E. and Giorgi, F., (2022). A Combined Hydrological and Hydraulic Modelling Approach for the Flood Hazard Mapping of the Po River Basin. *Journal of Flood Risk Management*, Vol.15. https://doi.org/10.1111/jfr3.12755.

[41] Sidek, L. M., Jaafar, A. S., Majid, W. H., Basri, H., Marufuzzaman, M., Fared, M. M. and Moon, W. C., (2021). High-Resolution Hydrological-Hydraulic Modeling of Urban Floods Using InfoWorks ICM. *Sustainability*, Vol.13. https://doi.org/10.3390/su131810259.

[42] Cohen, S., Brakenridge, G. R., Kettner, A., Bates, B., Nelson, J., McDonald, R., Huang, Y. F., Munasinghe, D. and Zhang, J., (2018). Estimating Floodwater Depths from Flood Inundation Maps and Topography. *JAWRA Journal of the American Water Resources Association*, Vol. 54, 847-858. https://doi.org/10.1111/1752-1688.12609.

[43] Peter, B. G., Cohen, S., Lucey, R., Munasinghe, D., Raney, A. and Brakenridge, G. R., (2022). Google Earth Engine Implementation of the Floodwater Depth Estimation Tool (FwDET-GEE) for Rapid and Large Scale Flood Analysis. *IEEE Geoscience and Remote Sensing Letters*, Vol. 19, 1-5. https://doi.org/10.1109/LGRS.2020.3031190.